Profiling of *Burkholderia pseudomallei* variants derived from Queensland's clinical isolates

Pauline M.L. Coulon[1], Kay Ramsay[2], Aven Lee[3], Edita Ritmejeryte[3], Miranda E. Pitt[1,4], Joyce To[1], Daniel G. Mediati[1], Sarah Reed[3], Patrick N. A. Harris[2] and Garry S.A. Myers[1]

Affiliations:

[1]Australian Institute for Microbiology and Infection, Faculty of Science, University of Technology Sydney, Ultimo, NSW, Australia

[2] The University of Queensland Centre for Clinical Research (UQCCR), Faculty of Medicine, The University of Queensland, Queensland, Australia

[3]Mass Spectrometry Facility, University of Queensland, Centre for Clinical Research, Queensland, Australia

[4] Department of Microbiology and Immunology, Doherty Institute, University of Melbourne, Victoria, Australia

Corresponding author:

Pauline M.L. Coulon, Australian Institute for Microbiology and Infection, Faculty of Science, University of Technology Sydney, NSW, Australia, +61390353555, pauline.coulon@uts.edu.au

Abstract

Burkholderia pseudomallei (*Bp*), an environmental bacterium and opportunistic pathogen endemic to tropical regions, is highly adaptive and thrives in diverse environments, from soil to human hosts. Bacterial adaptation is critical for survival, virulence modulation, and persistence during infection and can manifest as colony morphotype variation (CMV). Here, we characterized five clinical Bp isolates exhibiting heterogeneous populations with mucoid and non-mucoid colony morphologies. We used phenotypic assays, whole-genome sequencing, and proteomics to investigate the molecular pathways impacted by CMV - by comparing smooth and rough morphotypes. While phenotypic differences in protease activity, hemolysis, mucoidy, iron uptake and antibiotic sensitivity were rare, these traits alone could not distinguish morphotypes or group of isolates. Genomic comparisons revealed either no differences or limited isolate-specific mutations, which likely does not explain the overall difference in phenotypes. In contrast, proteomic analysis uncovered consistent shifts in protein abundance related to virulence, including quorum sensing, DNA methylation, and secretion systems. These findings suggest that CMV is driven by phase variation and regulatory mechanisms rather than punctual genomic modifications. Our proof-of-concept study underscores the limitations of phenotype or genome-based classification alone in the context of CMV and highlights the value of integrated multi-omics approaches to uncover CMV-associated biomarkers, with potential applications in diagnostics and the development of targeted therapies against persistent and drug-resistant Bp infections.

Importance

Burkholderia pseudomallei (Bp), the causative agent of melioidosis, is endemic to Australia, Asia, Africa, and the Americas. It predominantly affects Indigenous populations and individuals with diabetes, chronic lung or kidney disease, or alcoholism. Bp is known for its

exceptional genomic and phenotypic plasticity, enabling rapid adaptation to diverse environments. This adaptability is reflected by colony morphotype variation (CMV), including reversible phase variation between smooth and rough colonies. In this study, we report rough and smooth colonies from clinical samples and emphasize the importance of characterizing CMV through multi-omics approaches rather than relying solely on genomics and phenotypic traits. By integrating genomics, phenotypic and proteomic data, we identified that a limited number of mutations—including one in a putative regulatory element—likely drive major molecular changes between morphotypes. These affect the expression of quorum sensing (QS) systems, the transcriptional regulator ScmR, DNA methyltransferase, and virulence-associated genes.

Keywords: colony morphotype variation, epigenetics, quorum sensing, omics, regulatory elements, secretion systems

Introduction

Burkholderia are highly adaptable Gram-negative environmental saprophyte bacteria found in diverse ecological niches ranging from soil and plant roots to human hosts. Their remarkable phenotypic plasticity enables them to persist in various ecological niches, often facilitated by transmission through contaminated water, soil, and products (1-7). Among them, *Burkholderia pseudomallei* (*Bp*) poses a significant public health threat as the causative agent of melioidosis, a severe and often fatal disease in animals and humans (1, 8). While *Bp* is endemic to tropical and sub-tropical regions of Asia, Africa, Central and South America and Australia (1), it has been recognized since 2023 as naturally established in the environment of the United States (9).

Although most healthy individuals exposed to *Bp* do not develop melioidosis, vulnerable population with underlying conditions such as cystic fibrosis, diabetes, chronic kidney disease, chronic lung disease, alcoholism or with a compromised immune system often -are the most at risks. In these individuals, *Bp* infections can cause skin abscesses or severe pneumonia, often leading to fatal sepsis with a mortality rate reaching up to 52% (1, 10-17). The incidence of *Bp* infections is strongly correlated with heavy rains and flooding, and cases are expected to increase as climate change intensifies extreme weather events (18). In mid-2025, Queensland (Australia), reports it worst year of melioidosis in three decades with over 230 cases and 31 deaths (ABC News). Additionally, there is a growing concern that melioidosis cases could (1) spread into New South Wales (Australia), where the disease is less recognised by healthcare providers and (2) be transmitted directly by pets, livestock or wild animals through contact with infected wounds or via shared environment–even if no zoonotic transmission have been confirmed to date (7News)(8).

Burkholderia's rapid adaptation to environmental changes and stressors is often associated with modifications in outer membrane proteins, antibiotic production, and virulence factors (19-23). This adaptability is reflected by colony morphotype variation (CMV), a process by which bacteria switch between distinct colony morphologies. Although CMV plays a critical role in persistence during infection, it remains underexplored (24). A few studies have shown that CMV can result in mutations in global regulators, two-component systems, genome reduction and duplication, bacteriophage cluster integration and DNA methylation, as reviewed by Coulon and colleagues (24).

Among *Burkholderia* species, *Bp* has been the most extensively studied in terms of CMV. Chantratita and colleagues identified up to seven dynamic and reversible colony morphologies in *Bp* (19). Under laboratory conditions, these variants emerge in response to stress conditions and revert to the parental morphotype once the stress is removed (19, 22, 25). Notably, CMVs also occur during infection: in 10% out of over 450 clinical *Bp* isolates, a mixed mucoid and non-mucoid CMV population was observed on blood agar. The mucoidy phenotype was attributed to a difference in O-antigen Lipopolysaccharides (LPS; [OPS]) production, while no mutations or altered expression of the *wbiA* O-antigen acetylase was linked (26). Further, the emergence of small-colony variants (SCVs) from a wrinkled *Bp* isolate during long-term infections in murine was attributed to upregulation of the LPS biosynthesis cluster genes (27, 28). Using experimental evolution in the same model, Gierok and colleagues have demonstrated the emergence of two reversible yellow colony variants (YA and YB) from the environmental *Bp* K96243. These variants showed upregulation of the σ-54 dependent regulator *yelR*, leading to resistance to hypoxic stress and enhanced colonization and persistence in the murine stomach (29).

In this study, we characterised five additional *Bp* isolates undergoing CMV using phenotypic, genomic, and proteomic profiling to uncover the similarities and dissimilarities in molecular pathways impacted by CMV.

Ethical Approval

This study received ethical approval from the Royal Brisbane and Women's Hospital Ethics Committee (LNR/2020/QRBW/65573), with site-specific authority obtained from the Townsville Hospital and Health Service and approval under the Queensland Public Health Act.

Material and Method

Colony morphology screening

Briefly, ~200 Bp isolates were collected from Townsville between 1999 and 2020, and ~80 isolates were characterized as "mixed population" (30). Among the isolates listed in **Table S1**, each was streaked on Luria Broth (LB) agar plates containing 0.01% Congo red (CRLA) from -80°C stock and incubated at 37°C for three overnights – to confirm the mixed population phenotype.

Phenotypic assays

Production of virulence factors. Individual colonies (four biological replicates) were picked and stabbed into LB agar plate containing 1.5% skimmed milk to assess proteolytic activity (31); 0.5 g/L yeast extract supplemented with 4g/L D-mannitol (YEM) and agar to assess mucoidy (32); a modified recipe of Chrome Azurol S agar (using 10X chelated LB instead of minimal media 9 supplemented with chelated casamino acid) to assess siderophore production (33) and ensure the growth of clinical isolates; and Columbian horse blood agar

plate to assess hemolysis activity (34). Plates were incubated at 37°C for 3 days. Inhibition circles were measured and confirmed by statistical analyses (see specific text in the legend of Table 1).

Antimicrobial sensitivity assay. Individual colonies were resuspended in 0.9% NaCl solution to achieve a turbidity of 0.5-0.63 McFarland. Each bacterial suspension was then spread on Muller Hinton II agar plates to assess susceptibility to Meropenem using gradient MIC test strips (ETEST, range0.002-32 µg/mL; Biomérieux), and disk diffusion for Ceftazidime (10µg) and Sulphamethoxazole-Trimethoprim (25µg) (Oxoid). Antimicrobial susceptibility was determined according to EUCAST guidelines (v15). For CMVs from the same isolate showing considerable visual changes in antibiotic susceptibility, three biological replicates were conducted on independent days, and the average inhibition zone diameters were used for susceptibility classification.

Genomic analysis

gDNA extraction. Genomic DNA was extracted from a macrocolony grown for three nights at 37 °C on CRLA using either gDNA spin or high molecular weight extraction kits (NEB). Short-read sequencing (Illumina) was conducted on all CMVs. Briefly, libraries were prepared using 1 ng of gDNA via the Nextera XT kit and sequenced using the NovaSeq XPlus platform (35). On select isolates, long-read sequencing (Oxford Nanopore Technologies) was implemented. Libraries were prepared using 400 ng gDNA with the SQK-NBD114.24 kit and sequenced using R10.4.1 flow cells on the GridION platform. Reads were base-called using Dorado 7.6.7.

Genome assembly. Nanopore and Illumina reads were quality-filtered and trimmed using Nanofilt (v.2.8.0; (36)) and fastp (v0.24.1; (37)) respectively. Nanopore reads were

assembled using Autocycler (v0.4.0; (38)). Assemblies were polished using Polypolish (v0.6.0; (39)) and then POLCA from the pypolca toolkit (v3.0.1; (40)) with Illumina reads. Final assemblies were annotated using Bakta (v1.11; (41)). For the second CMV from each isolate, Illumina reads were assembled into contigs using Unicycler (short read option, v.0.5.1; (42)).

Genomic modification analyses. To identify SNPs and indels, Illumina reads from the second CMV were mapped onto the corresponding first CMV assembly using Snippy (v4.6.0, haploid mode; - Galaxy implementation) (43). As a control, Illumina reads from the first CMV were also mapped onto their own assemblies, confirming the absence of variation.

Prediction of regulatory targets in non-coding regions. At least 50-nt of the upstream and downstream sequences of non-coding genomic variants (including SNPs, insertions or deletions) were extracted and used as input into IntaRNA (44) to predict regulatory targets in *Bp*. RNA-RNA interactions were filtered for those occurring within 50-nt upstream and 25-nt downstream of mRNA start codons (AUG), at least 7 nucleotides of base-pairing, and containing no G-U base-pairs at the 5’ or 3’ seed ends.

Prediction of secondary structure in non-coding regions. The non-coding genomic variant regions (50-nt upstream and downstream, as *above*) were extracted and used as input into the RNAfold software package to calculate the minimum free energy secondary structure formation of sequences(45). The analyses were performed using the -p, -d2, and --noLP default parameters.

Identification of genes encoding for DNA methyltransferase and their linked motifs. Pod5 files obtained from Nanopore sequencing were merged, using pod5 merge function and analyzed for DNA methylation motifs using the Dorado with both dna_r10.4.1_e8.2_400bps_hac@v4.3.0_6mA@v2, dna_r10.4.1_e8.2_400bps_hac@v4.3.0_5mC_5hmC@v1 models (https://github.com/nanoporetech/dorado). To identify the location and number of detected motifs, as well as the genes encoding DNA methyltransferases, the call_methylation and annotate_rm functions from MicrobeMod were used. These tools were provided with the corresponding genome assembly ".fasta" and annotation ".gff3" files for each isolate (**Table S3-4**).

Proteomic analysis

Protein extraction and peptide preparation. Bacteria cells in 1M Tris-HCL containing 1% SDS were sonicated in an ultrasonic bath YJ5120-1 (Labtex) for 3 minutes, followed shaking at 1,000 rpm at 95°C for 15 minutes on a Thermomixer Compact (Eppendorf). The mixture was allowed to cool down to room temperature and 30 µL was mixed with 270 µL of Buffer I (6 M guanidine chloride, 50 mM Tris pH 8.0, 10 mM DTT) and incubated at 30°C for 40 min. Following addition of 9 µL of 0.5 M iodoacetamide, the sample was incubated at 30°C for 50 min. The reduced and alkylated protein sample was transferred to a 10 kDa cut-off Amicon Ultra device (Merck) which was placed into a collection tube and centrifuged at 14,000 × *g* for 30 min. The flow-through from the column was removed and 300 µL of 100 mM ammonium bicarbonate was added to the column followed by centrifugation at 14,000 × *g* for 30 min. To digest proteins in the column, 130 µl of 100 mM ammonium bicarbonate containing 2 µg Trypsin was added. The column was incubated at 37°C for 24 h and then centrifuged in a new collection tube at 14,000 × *g* for 30 min. Fifty µL of water with 0.1%

formic acid was then added to the spin column followed by centrifugation at 14,000 × *g* for 30 min to elute the remaining digested peptides. Enzymes and salts were removed using C_{18} ZipTips (Merck) following the manufacturer's instructions and desalted peptides were eluted with 80% acetonitrile/0.1% formic acid into microcentrifuge tubes. Digested peptide samples were dried down using a vacuum concentrator (Concentrator plus, Eppendorf) and reconstituted with 50 µL water with 0.1% formic acid prior to LC-MS/MS analysis.

LC-MS/MS analysis. The samples were chromatographically separated and resulting proteomics data was acquired using an Acquity M-class micro-LC system (Waters, USA) coupled with ZenoTOF 7600 LC-MS/MS system using the OptiFlow Turbo V ion source. (AB Sciex). Two µL of sample were loaded onto Micro TRAP C18 column (0.3 × 10 mm; Phenomenex) and washed for 10 min at 10 µL/min with 97% solvent A (water with 0.1% [v/v] formic acid) and 3% solvent B (99.9% [v/v] acetonitrile, 0.1% [v/v] formic acid). Liquid chromatography was performed at 5 µL/min using a 2.7 µm Peptide C18 160Å; (0.3 × 150 mm; Bioshell) column with the column oven temperature maintained at 40°C. The gradient started at 3% solvent B which was increased to 5% by 0.5 min, followed by an increase to 35% solvent B by 38.9 min and then another increase to 80% solvent B by 39 min. The column was washed with 80% solvent B for 3.9 min before equilibrating with 3% solvent B from 43 to 45 min. Data was acquired using Zeno SWATH DIA, using a 65 variable width SWATH windows. The TOF MS parameters were as follows: precursor mass range was 400 – 1500 m/z; declustering potential (DP) was set to 80 V and accumulation time was set at 0.25 s. The TOF MS/MS parameters were as follows: fragmentation mass range was set to 100 – 1500 m/z; with an accumulation time of 0.025s; fragmentation mode was set to CID with Zeno pulsing selected. The collision energy for the MS/MS acquisition was automatically adjusted according to the m/z and charge of the peptide.

Data analyses. Raw label free quantification (LFQ) LC-MS/MS data were converted to .mzML files, using MS convert, to allow the data search using Fragpipe v22 (46). Protein identification was conducted against the respective annotated proteomes using the DIA_SpecLib_Quant workflow, which builds a spectral library with MSFragger-DIA and performs quantification with DIA-NN. The output "diann-output.pg_matrix.tsv" was filtered to remove contaminants and retain proteins with at least two non-missing values for at least one group. Data was normalized using the variance stabilization normalization (47). Proteins with two or more missing values in one group were categorized as "detected/not detected." For proteins with a single missing value in one group, missing data were imputed using the mean of the other replicates in that group. Differential protein expression between groups was assessed using Welch's t-test, with Benjamini–Hochberg correction applied to control the false discovery rate (adjusted $p < 0.05$) (48, 49). Analyses were performed on three biological replicates (Table S5-9).

Proteomic representation. All differences in protein abundances observed among the Townsville *Bp* isolates in this study were mapped back to the reference strain *Bp* K96243, widely regarded as the model organism for Bp research and the basis for most virulence factor and pathway annotations. To identify homologous proteins between the Townsville Bp isolates and Bp K96243, a megablastp was set up with only one output match for each gene in query using the following parameters: -evalue 10 -outfmt 6 -num_threads 3 -max_target_seqs 1 -max_hsps 1 (Table S10; (50). Clustering of orthologous groups (COGs) for annotated proteins were determined using EggNOG tool v5 (Table S11; (51)). Heatmap representation, made using 'pheatmap' package in R (52), was based on protein with at least

two isolates showing differences with either three not detected by LC-MS/MS or with maximum two not differential abundance between CMV.

Multi-omics integration

Principal component analysis. Data were transformed using binary variable to be able to create a principal component analysis using 'stats' R package function 'prcomp' (53). PCA was conducted separately for each omics layer using, respectively 16 phenotypes, 19 genomic top 30 proteomic variables. For integrative analysis, all genomic and phenotypic variables, along with the top 30 most variable proteomic features, were combined to explore multi-omics clustering patterns across isolates and colony morphotypes.

Data availability

Genomes from this study are available in GenBank under the Bioproject: PRJNA1295092 (54, 55). Proteomic raw data deposited to the ProteomeXchange Consortium via the PRIDE partner repository with the dataset identifier PXD065768 (56).

Results

As expected, phenotypic profile do not cluster by colony morphotype

Among over 200 clinical Bp isolates from their Townsville collection (30), Etipola and colleagues (unpublished) classified them into wrinkled, mucoid, or mixed colony morphotypes when grown on Ashdown selective agar. From the group classified as having

"mixed" morphologies, we selected seven wrinkled clinical isolates and their corresponding mucoid variants for further genomic, proteomic, and phenotypic investigation (**Table S1**). Since CMV can occur spontaneously under laboratory conditions – such as removing antibiotic pressure (19, 22, 25) – we streaked each isolate onto CRLA to confirm its capacity to generate variants.

Isolates TSV267 and TSV274 produced only one type of colony morphology on CRLA. Therefore, the five remaining isolates (TSV82, 140, 268, 270 and 287) were selected for further characterization. To confirm morphology differences, parental and variants were also grown on Ashdown agar (**Fig. 1**). Interestingly, TSV82, TSV268, and TSV287 smooth variants were consistently classified as type SI on CRLA and type II (TSV82 and TSV287 smooth) and type I (TSV268 smooth) on Ashdown agar, whereas their respective rough CMV forms were further differentiated. On CRLA, TSV82 and TSV268 rough variants were classified as RI, and TSV287 rough as SI. On Ashdown, these rough variants were more distinct, with TSV82 rough classified as type VIII, TSV268 rough as type II, and TSV287 rough as type VII. In contrast, TSV140 and TSV270 smooth variants were classified as SI on CRLA and type II and III on Ashdown, respectively, while their rough forms were more divergent: TSV140 rough was RII on CRLA and type V on Ashdown, and TSV270 rough was RIII on CRLA and type V on Ashdown (19, 57). With extended incubation, some morphotypes shifted (**Figure 1B**). TSV270 rough on CRLA developed a lighter inner colony, while TSV268 smooth lost its wrinkled texture and became fully smooth.

Since CMV often reflects underlying adaptive phenotypes, we next assessed virulence-associated traits, including proteolytic and hemolytic activity, mucoidy, and antibiotic susceptibility (**Table 1**). All ten rough and smooth CMVs were sensitive to meropenem (MEM), ceftazimidime (CAZ). However, while all ten rough CMVs were sensitive to TMP-SMX, the smooth variant of TSV140 was resistant, whereas the smooth variant of TSV268

remained classified as 'Susceptible, Increased Exposure' but was more sensitive than its rough counterpart.

As expected, smooth variants were generally more mucoid on YEM agar than their respective rough parental forms. Additionally, rough variants of TSV82, TSV270, and TSV287 displayed hemolytic activity, in contrast to their smooth counterparts. TSV82 and TSV270 rough forms also produced significantly more protease and siderophore than the smooth forms, while TSV287 rough only displayed a higher production of siderophore compared to its smooth variant.

Table 1 1 Phenotypic profiling of seven Bp clinical isolates and their respective mucoid variants

Isolate	Colony morphology	Antibiotic Susceptibility test			Mucoidy	Hemolysis	Proteolytic Activity (cm^2)	Siderophore Production (cm^2)
		MEM	CAZ	TMP-SMX				
TSV 82	rough	S	I	I	-	beta	1.81 ± 0.51 *	7.473 ± 1.239*
	smooth	S	I	I	++	gamma	0.89 ± 0.09	5.097 ± 0.911
TSV 140	rough	S	I	I	+	gamma	0.73 ± 0.10	4.113 ± 0.728
	smooth	S	I	R	++	gamma	0.71 ± 0.00	4.634 ± 1.237
TSV 268	rough	S	I	I	-	gamma	0.00 ± 0.00	2.058 ± 0.548
	smooth	S	I	I	+	gamma	0.00 ± 0.00	2.307 ± 0.288
TSV 270	rough	S	I	I	+	beta	1.80 ± 0.23 **	13.888 ± 2.865**
	smooth	S	I	I	++	gamma	0.64 ± 0.07	3.753 ± 1.46
TSV 287	rough	S	I	I	-	beta	0.75 ± 0.10	7.707 ± 0.999*
	smooth	S	I	I	+	gamma	0.92 ± 0.13	5.6 ± 0.916

EUCAST: S = Susceptible; I= Susceptible increased exposure; R= Resistant; Meropenem (MEM): S<=2; R>2; Ceftazidime (CAZ; disk 10µg): I<=50mm; R<18mm; Trimethoprim-Sulphamethadoxone (TMP-SMX; disk 1.25-23.75µg): S>=50mm; R<17mm; susceptibility statistically different.

Mucoidy: - = non-mucoid; + = mucoid; ++ = more mucoid; Hemolysis: beta = complete lysis of red blood cell; gamma = no lysis; Proteolytic activity: Mean ± Stand deviation. * = p value <0.05; ** = 0.01<p value<0.05; comparison TSV 270 rough vs smooth by ttest and TSV 82 rough vs smooth by wilcoxon test; Siderophore production: Mean ± Stand deviation. * = p value <0.05; ** = 0.01<p value<0.05; comparison by ttest.

To further explore CMV, we assessed the formation of sectors, reflecting in variant emergence, after extended incubation on each medium (**Fig. 1B**). CRLA induced smooth variants in the initial rough forms of TSV268 and TSV270, while blood agar promoted smooth variants in the rough forms of TSV82, TSV268, and TSV287 but also in the smooth form of TSV82. Ashdown agar triggered morphotype changes only in TSV82 and TSV287. Finally, TSV82 smooth variants emerged from its initial rough form on LB agar supplement with skimmed milk. TSV140 showed no variant emergence across any media.

Taken together, these results demonstrate that Bp colony morphology varies across some media but does not reliably correlate with virulence-related phenotypes.

Genomic analyses reveal distinct mutations including in noncoding region with potential predicted regulatory elements

After confirming that both rough and smooth colony morphotype from each isolate shared the same sequence type (ST; **Table S1**), we investigated whether differences in colony morphology were due to underlying genomic variations. We first assembled the genome of TSV82 rough, TSV 140, TSV268, TSV270 and TSV270 smooth colonies and mapped Illumina reads from TSV82 smooth, TSV140, TSV268, TSV270 and TSV270 rough on their respective counterparts assembled genomes using Snippy (**Table 2**).

Table 2: Genomic modifications between rough and smooth CMV

Comparison	Average of illumina coverage	Chromosome	Position	Type	Reference	Alternative	Evidence	Frame Type	Effect	Locustag	Gene	Product	Bp K9623 locustag
TSV82 Smooth vs Rough	Contig 1 50.5X Contig 2 41.4X	1	87085	snp	G	A	A:39 G:3	CDS	synonymous c.3825G>A p.Thr1275Thr	RS_00350	*mbaJ*	siderophore related no-ribosomal peptide synthase	BPSL1778
		1	87236	snp	T	C	C:42 T:2	CDS	synonymous c.3976T>C p.Leu1326Leu				
		1	87274	snp	C	A	A:40 C:1	CDS	missense c.4014C>A p.His1338Gln				
		1	87454	snp	C	T	T:50 C:1	CDS	synonymous c.4194C>T p.Ile1398Ile				
		1	88446	snp	C	T	T:16 C:1	CDS	missense c.5186C>T p.Ala1729Val				
		1	88575	snp	A	C	C:21 A:2	CDS	missense c.5315A>C p.Asp1772Ala				
		1	88933	snp	C	T	T:16 C:1	CDS	synonymous c.5673C>T p.Arg1891Arg				
		1	89173	snp	G	A	A:24 G:2	CDS	synonymous_ c.5913G>A p.Glu1971Glu				
		1	89512	snp	C	A	A:20 C:1	CDS	synonymous c.6252C>A p.Ala2084Ala				
		1	153859	snp	T	A	A:28 T:2	CDS	missense c.167A>T p.His56Leu	RS_00580		AMP-binding domain protein	BPSL1734
		1	991823	snp	A	T	T:13 A:1	CDS	missense c.217A>T p.Thr73Ser	RS_04110		Oxidoreductase, FAD-binding family protein	BPSL2405
		1	2552774	del	CG	C	C:54 CG:4	intergenic region				Putative non coding region with regulatory element in 5' RS_11330	BPSL0367
		1	2942569	snp	G	A	A:10 G:0	CDS	synonymous c.636G>A p.Ala212Ala	RS_12950		Phosphoribosyl transferase	BPSL0718
		1	2942620	snp	C	G	G:10 C:0	CDS	synonymous c.687C>G p.Ala229Ala				
		1	2942657	snp	G	A	A:15 G:0						
		2	262512	snp	T	C	C:27 T:2	CDS	missense c.628A>G p.Lys210Glu	RS_18625		DNA-binding protein	BPSS0830
		2	486060	snp	G	A	A:28 G:1	CDS	missense c.601G>A p.Glu201Lys	RS_19540		SDR family NAD(P)-dependent oxidoreductase	BPSS1007
		2	537160	complex	GGCCGG	AATCGA	AATCGA:10 GGCCGG:0	CDS	missense c.869_874delCCGGCCinsTCGATT p.ProGlyPro290LeuAspSer	RS_19610		Helix-turn-helix domain protein putative AraC family members	BPSS1020
		2	538080	snp	G	T	T:16 G:1	intergenic region				Putative non coding region with regulatory elementin 5' RS_19610	
		2	547475	snp	C	A	A:16 C:1	CDS	synonymous c.285G>T p.Ala95Ala	RS_19655		Branched-chain amino acid ABC transporter permease	BPSS1030
		2	685277	snp	G	A	A:29 G:1	CDS	missense c.194C>T p.Ala65Val	RS_20305	*hyfB*	hydrogenase 4 subunit B	BPSS1147
		2	737147	snp	A	G	G:30 A:2						
		2	746638	snp	A	G	G:30 A:0	CDS	synonymous c.783T>C p.Ser261Ser	RS_20510		Luciferase oxidoreductase, group 1 family protein	BPSS1190
		2	988639	snp	A	G	G:55 A:4	CDS	missense c.164A>G p.Gln55Arg	RS_21370		Peptidase, S9A (Prolyl	BPSS1346

												oligopeptidase) family	
		2	1313262	snp	C	T	T:12 C:0	CDS	synonymous c.207C>T p.Ile69Ile	RS_22655		PPC domain-containing protein	BPSS1588
		2	1791476	snp	C	T	T:22 C:1	CDS	synonymous c.2052C>T p.Ala684Ala	RS_24525	*rbbA*	ribosome-associated ATPase/putative transporter RbbA	BPSS1938
		2	2200644	snp	G	T	T:20 G:1	intergenic region				Putative non coding region with regulatory elementin 5' RS_26200	BPSS2260
		2	3013633	snp	G	C	C:69 G:0	CDS	synonymous c.30C>G p.Ala10Ala	RS_29435	*potI*	ABC-type spermidine/putrescine transport system, permease component II	BPSS0464
		2	3015293	snp	A	G	G:38 A:2	CDS	synonymous c.492T>C p.Arg164Arg	RS_29445	*potG*	Spermidine/putrescine import ATP-binding protein	BPSS0466
		2	3015662	snp	A	G	G:37 A:1	CDS	synonymous. 123T>C p.Ala41Ala				
		2	3016583	snp	G	C	C:53 G:4	CDS	synonymous c.513C>G p.Ala171Ala	RS_29450	*potF*	Putrescine-binding periplasmic protein	BPSS0467
		2	3016945	snp	G	A	A:47 G:1	CDS	missense c.151C>T p.Pro51Ser				
		2	3017125	snp	G	A	A:24 G:0	promotor					
TSV140 Rough vs Smooth	Contig 1 67.8X Contig 2 69.8X Contig 3 90X	2	2170684	del	AGCTTCG	A	A:10 AGCTTCG:0	CDS	missense c.53_58delAGCTTCG p.PheGly103Phe	RS_30990		serine/arginine repetitive matrix 1 CDS	BPSS1650
TSV268 Rough vs Smooth	Contig 1 55.7X Contig 2 56.7X	-											
TSV270_Rough vs Smooth	Contig 1 74X Contig 2 76.3X	-											
TSV287 Rough vs Smooth	Contig 1 64.6X Contig 2 55.4X	1	774690	del	GACGAATCAGT	G	G:32 GACGAATCAGT:0	intergenic region		RS_03535		Putative non coding region with regulatory elementbetween 3' ispA (RS_03530) and 5' trnP tRNA (RS_03540)	BPSL3006-BPSL3007

Firstly, no genomic variation was detected between the rough and smooth forms of TSV268 and TSV270, suggesting that their CMV is likely driven by phase variation. In contrast, TSV82 smooth differed from its rough counterpart by 33 mutations including four in intergenic regions, 16 synonymous and eleven missenses. To confirm the accuracy of these mutations, we mapped contigs from the TSV82 smooth Illumina assembly onto the TSV82 rough reference to ensure they were not artifacts associated with contig ends. However, the Illumina coverage was 50.5× for contig 1 and 41.4× for contig 2, which could account for the observed mutations (**Table 2**).

We then assessed the predicted impact of intergenic and missense mutations based on amino acid substitution significance and genomic context (e.g., within open reading frames or promoter regions). MbaJ, part of the siderophore biosynthesis cluster (which could explain the observed difference in siderophore production for this isolate; **Table 1 and Fig. S1A**); PotF, a periplasmic binding protein of the PotFGHI system involved in putrescine import in *E. coli* (**Fig. S1B**); TSV82_RS_18625/BPSS0830, a DNA-binding protein; a NAD(P)-dependent oxidoreductase (**Fig. S1C**); and TSV82_RS_19610/BPSS0120, a helix-turn-helix domain-containing protein and putative member of the AraC family of transcriptional regulators (**Fig. S1D**). To evaluate the potential structural consequences of these mutations, we used AlphaFold 4 to predict and align the tertiary structures of wild-type and mutated proteins. Mutations were either located in regions with low prediction confidence or did not significantly alter predicted secondary or tertiary structures (**Fig. S1**). Further experimental validation will be necessary to assess their functional impact. Finally, we identified mutations between smooth and rough colonies within predicted ncRNAs located in the 5′ untranslated regions (UTRs) of TSV82_RS_19610 (a G-to-T substitution), TSV82_RS_11330 (a deletion of “CG”), and TSV82_RS_26200 (a G-to-T substitution).

For TSV140, TSV140 rough and smooth variants differed by a deletion of one set of "GCTTCG" repeat sequence within TSV140_RS_30990 encoding for a putative serine/arginine repetitive matrix 1 (**Table 2**). This deletion induces a frame shift resulting in a putative truncated protein. In TSV287, the rough variant lacked one "ACGAATCAGT" repeat between the 3' UTR of *ispA* (TSV287_RS_03530) and 5' UTR *trnP* tRNA (TSV287_RS_03535) (**Table 2**).

Proteomic profile of *Bp* isolates and their CMVs reveal alterations in proteins involved in virulence, quorum sensing and DNA methylation

In this study, we assessed phenotypes associated with key virulence factors known as essential for *Bp* pathogenicity, including protease, siderophore and EPS production, along with susceptibility to antibiotics commonly used for melioidosis treatment. However, *Bp* is also known to modulate its production of lipopolysaccharide (LPS) and capsular polysaccharide (CPS) to escape host immunity, resistance to antibiotic and phage attack, employ multiple secretion systems to invade within macrophages (to replicate) and then escape (58-68). To gain deeper insights on the molecular pathways affected by CMV, we performed proteomic analyses comparing smooth and rough colony morphologies when grown on CRLA plates for 3 days (**Fig. 2; Tables S4-10**). Differential abundance was observed in proteins involved in a wide range of biological functions including amino acid and carbohydrate metabolism and transport, cell cycle control and division, cell wall/membrane/envelope biogenesis, defense mechanisms, energy production and conversion, inorganic ion transport and metabolism, lipid metabolism, nucleotide metabolism, post-translational modification and chaperone function, secondary structure, signal transduction, transcription, and translation. These proteins were consistently either undetected or significantly lower or higher in abundance in at least three smooth colonies

compared to their rough counterparts. Notably, proteins associated with cell motility and intracellular trafficking, and secretion were typically undetected or present in lower abundance in rough colonies relative to smooth colonies.

More specifically, proteins involved in the CAC^{6}AG DNA methylation motif (**Table S2-3**), antimicrobial resistance (PenA, AmrR), bactobolin biosynthesis (BtaN, L, H, J, Q), haem uptake (BhuS, T, V), CPS biosynthesis (WbcN), chemotaxis (CheR, CheD), flagellar biosynthesis (FliN, G, FlgG, H, K FlhA, FliD, H, I, J, O, S, P), Macrophage infectivity potentiators (Mip2), Malleilactone and malleicyprol biosynthesis (MalB, I, M), Malleobactin synthesis (FmtA, MbaI, F, A), Pyochelin biosynthesis (FptA, PchA, B, C, D, G, H, I,) T3SS-3 secretion system (BprQ), T6SS-1 secretion system (TssD-5 aka Hcp1), two-component signal transduction system (BprR), Type II-OPS biosynthesis (Wzt) are not detected or in lower abundance in rough colonies relative to smooth colonies. In contrast, proteins involved in bacterial cellulose synthase (BcsA), EPS cepacian cluster I and II (BceA, C, D, E, F, G, H, N, M, R, T), quorum sensing (BpsI3/R3 and ScmR), T3SS-3 cascade regulator BspR, T6SS-6 (TagM-1, lipoprotein), Type III O−PS polysaccharide (e.g.: RbfbF, G, H) Type IV pilus biosynthesis (PilS), were not detected or in lower abundance in smooth colony when compared to rough colonies (**Fig. 2; Tables S4-10**).

Altogether, these results indicate that CMV significantly affects the expression of numerous proteins involved in virulence, including those associated with quorum sensing and DNA methylation. While these findings highlight the importance of CMV in modulating virulence, further studies are required to determine whether ScmR, quorum sensing, and DNA methylation directly regulate CMV and associated modulation of virulence factor production.

Mutations in non-coding regulatory elements may contribute to differential protein abundance, but are unlikely to drive CMV

Given the identification of mutations in non-coding intergenic regions that may contain regulatory elements such as small (s)RNA (with their predicted structure in **Fig. S2**), we investigated whether these regulatory elements could account for the observed differential protein expression (**Table S11**). Firstly, none of the potential predicted ncRNA had been previously reported (69, 70). Target prediction linked these predicted ncRNAs to genes involved in Type III (*bsaV, bsaK*) and Type IV (*vgrG, bimA*) secretion systems, antimicrobial resistance (*penA*), capsular polysaccharide biosynthesis (*wcbK*), chemotaxis (*cheY*), and secondary metabolite biosynthesis (e.g., *pchD/E* for pyochelin, *malF/M* for malleilactone, *mbaE* for malleobactin, *bceQ* for EPS cepacian, and *bhuU* for Burkholderia haem uptake). However, most of these targets did not exhibit significant differences in protein abundance between rough and smooth colonies in our proteomic analyses. Thus, while the non-coding regions merit further investigation for potential regulatory elements, they do not appear to be the primary drivers of colony morphotype variation.

Deeper -omics profiling shows potential to better characterize *Bp* isolate

Identification based solely on phenotype is unreliable due to the inherent variation in *Burkholderia* colony morphotypes (19, 57), which is further complicated by CMV occurring within individual isolates as an adaptive response. Our combined phenotypic and genomic analyses revealed that these genomic modifications do not explain alone the observed changes (**Fig. 1, Table 2**). This was confirmed by principal component analysis (PCA), where phenotypic and genomic data failed to cluster similar morphotypes or isolates (**Fig. 3A**). In contrast, proteomic profiling allowed more consistent discrimination between rough and smooth CMV variants and even between distinct smooth variants (**Fig. 3A**).

However, proteomics alone lacks biological context without accompanying phenotypic data, particularly for virulence traits, pathogenicity, and responses to antimicrobial treatment or stress, which may also be shaped by spontaneous mutations. Therefore, integrating all

datasets provides the most biologically relevant insights (**Fig. 3B**). While smooth isolates are not further distinct by integrating phenotypic and genomic data, further rearrangements are observed between rough isolates.

Discussion

Bp has been previously reported to exhibit a heterogeneous population, with both mucoid and non-mucoid colonies, and to undergo CMV depending on the presence of environmental pressures. While genomic profiling is often used to study Bp adaptation during infection and phenotypic assays are used to characterize CMV, integrated studies examining the relationship between genomic changes, phenotypic shifts and proteomic alterations remain rare (24, 25, 71). In this study, we employed a multi-omics approach to investigate phenotypic, and proteomic changes associated with CMV, along with underlying genomic modifications. Our aim was to reveal both conserved and isolate-specific features associated with the switch between rough and smooth morphotypes – which might transition from an acute-like to a chronic-adapted state during infection (64).

In several isolates, phase variation appeared to drive the switch between rough and smooth colony morphologies in the absence of detectable genomic variation. In contrast, other isolates exhibited limited but notable genomic modifications. In TSV82, SNPs led to missense mutations in a protein involved in siderophore biosynthesis, along with changes in both the promoter region and ORF of potF, a gene encoding a potential protective antigen for melioidosis (72). However, it is important to note that the genomic variation observed in TSV82 may be partially attributed to lower Illumina read coverage (below 50×). Additionally, across TSV82 and TSV287 isolates, either a missing repeat sequence or a SNP was detected within a putative novel mRNA regulatory element (69, 70).

Predicted targets of the putative regulatory element suggest involvement in macrophage escape, giant multinucleated cell formation - possibly through predicted interacting with genes involvement in type III and IV secretion systems - and the regulation of several biosynthetic gene clusters linked to virulence and antimicrobial resistance - including those responsible for malleilactone, malleicyprol, malleobactin, and pyochelin biosynthesis. While some key regulators, such as BspR—known to regulate the T3SS-3 and influence T6SS-5—showed differential abundance in the proteomics analysis, other secretion system components remained unchanged. This suggests that further studies are needed to clarify the impact of CMV on both secretion systems, which are critical for macrophage invasion and intracellular survival during infection (58-67).

Nonetheless, our data show extensive changes in pathways related to flagella, antimicrobial molecules, siderophore biosynthesis, CPS, LPS, and OMPs involved in antimicrobial resistance. These findings support previous studies describing the emergence of SCVs in Bp through phase variation, as well as the role of genomic modifications in adaptation during chronic infection (17, 24, 73, 74). The limited number of point mutations observed suggests that while they may contribute to phenotypic changes, they are unlikely to be the primary drivers of CMV. If genomic modifications were the main cause, we would expect more extensive alterations across regulatory genes and isolates.

Instead, the broad phenotypic and molecular changes associated with CMV are more likely driven by global regulatory systems—such as ScmR, quorum sensing, and epigenetic mechanisms like DNA methylation. These pathways were affected at the protein level in our study. This aligns with previous work demonstrating that ScmR regulates virulence factor production and quorum sensing in *B. thailandensis*, a surrogate model of *Bp*, and that both quorum sensing and DNA methylation influence phase variation in *B. ambifaria*, a member of the *Burkholderia cepacia* complex (23, 75, 76).

This study aimed to serve as a preliminary investigation, ultimately demonstrating that integrating of multi-omics data —phenotypic, genomic, and proteomic— provides valuable insights into the biological impact of CMV. This approach allowed us to differentiate isolates by morphotype and to uncover mechanisms underlying bacterial adaptation. However, limitations remain, particularly in proteomic analyses, where LC-MS/MS detection thresholds may restrict peptide identification. Future work will involve expanding this approach to a broader collection of isolates from environmental, animal, and human sources, spanning acute and chronic infections. We aim to generate a comprehensive database that integrates multi-layered omics data, including epigenomics, transcriptomics and metabolomics, with virulence phenotypes (e.g., macrophage invasion and escape), antibiotic responses, and clinical outcomes. This will improve our ability to discover the various mechanisms underlying bacterial adaptation – visible through CMV - correlate molecular features with disease severity and persistence, and to identify stable biomarkers for diagnostic and therapeutic targets.

Acknowledgment

The authors thank Julien L. Breton-Robin for helping set command lines tools using singularity. This work was supported by the funding AIMI and UTS Faculty of Science seed fundings hold by Dr Pauline M.L. Coulon, the strategic research accelerator funding (SRA 2726229) hold by Prof Garry Myers and EL2 Investigator grant from the NHMRC (APP2033851) hold by Dr Patrick N.A. Harris. Part of this work was carried out during the award of a Chancellor’s Research Fellowship to Daniel G. Mediati. Experimental work was

done at UQCCR which would not have been possible without the ISME scholar funding awarded to Dr Pauline M.L. Coulon.

P.M.L.C: Concept and visualisation, Funding, Experimental work; D.G.M: Experimental work: data analyses and predictions; M.E.P and J.T: Experimental work: DNA libraries and sequencing; A.L, E.R and S.R: Experimental work: sample preparation and LCMS runs for the proteomic experiment; P.N.A.H: Reviewing and Funding; G.S.A.M: Reviewing and Funding.

References

1. Meumann EM, Limmathurotsakul D, Dunachie SJ, Wiersinga WJ, Currie BJ. 2024. *Burkholderia pseudomallei* and melioidosis. Nat Rev Microbiol 22:155-169.
2. Kunakom S, Eustaquio AS. 2019. *Burkholderia* as a Source of Natural Products. J Nat Prod 82:2018-2037.
3. Torbeck L, Raccasi D, Guilfoyle DE, Friedman RL, Hussong D. 2011. *Burkholderia cepacia*: This Decision Is Overdue. PDA J Pharm Sci Technol 65:535-43.
4. Cundell T. 2019. Excluding *Burkholderia cepacia* complex from aqueous, non-sterile drug products. American Pharmaceutical Review 22.
5. Tavares M, Kozak M, Balola A, Coutinho CP, Godinho CP, Hassan AA, Cooper VS, Sa-Correia I. 2020. Adaptation and Survival of *Burkholderia cepacia* and *B. contaminans* During Long-Term Incubation in Saline Solutions Containing Benzalkonium Chloride. Front Bioeng Biotechnol 8:630.
6. Gee JE, Bower WA, Kunkel A, Petras J, Gettings J, Bye M, Firestone M, Elrod MG, Liu L, Blaney DD, Zaldivar A, Raybern C, Ahmed FS, Honza H, Stonecipher S, O'Sullivan BJ, Lynfield R, Hunter M, Brennan S, Pavlick J, Gabel J, Drenzek C, Geller R, Lee C, Ritter JM, Zaki SR, Gulvik CA, Wilson WW, Beshearse E, Currie BJ, Webb JR, Weiner ZP, Negron ME, Hoffmaster AR. 2022. Multistate Outbreak of Melioidosis Associated with Imported Aromatherapy Spray. N Engl J Med 386:861-868.
7. McRobb E, Sarovich DS, Price EP, Kaestli M, Mayo M, Keim P, Currie BJ. 2015. Tracing melioidosis back to the source: using whole-genome sequencing to investigate an outbreak originating from a contaminated domestic water supply. J Clin Microbiol 53:1144-8.
8. Sprague LD, Neubauer H. 2004. Melioidosis in animals: a review on epizootiology, diagnosis and clinical presentation. J Vet Med B Infect Dis Vet Public Health 51:305-20.
9. Petras JK, Elrod MG, Ty MC, Dawson P, O'Laughlin K, Gee JE, Hanson J, Boutwell C, Ainsworth G, Beesley CA, Saile E, Tiller R, Gulvik CA, Ware D, Sokol T, Balsamo G, Taylor K, Salzer JS, Bower WA, Weiner ZP, Negron ME, Hoffmaster AR, Byers P. 2023. Locally Acquired Melioidosis Linked to Environment - Mississippi, 2020-2023. N Engl J Med 389:2355-2362.
10. Limmathurotsakul D, Golding N, Dance DA, Messina JP, Pigott DM, Moyes CL, Rolim DB, Bertherat E, Day NP, Peacock SJ, Hay SI. 2016. Predicted global distribution of *Burkholderia pseudomallei* and burden of melioidosis. Nat Microbiol 1.
11. Chantratita N, Phunpang R, Yarasai A, Dulsuk A, Yimthin T, Onofrey LA, Coston TD, Thiansukhon E, Chaisuksant S, Tanwisaid K, Chuananont S, Morakot C, Sangsa N, Chayangsu S, Silakun W, Buasi N, Chetchotisakd P, Day NP, Lertmemongkolchai G, West TE. 2023. Characteristics and One Year Outcomes of Melioidosis Patients in Northeastern Thailand: A Prospective, Multicenter Cohort Study. Lancet Reg Health Southeast Asia 9.
12. Currie BJ, Mayo M, Ward LM, Kaestli M, Meumann EM, Webb JR, Woerle C, Baird RW, Price RN, Marshall CS, Ralph AP, Spencer E, Davies J, Huffam SE, Janson S, Lynar S, Markey P, Krause VL, Anstey NM. 2021. The Darwin Prospective Melioidosis Study: a 30-year prospective, observational investigation. Lancet Infect Dis 21:1737-1746.

13. Currie BJ, Fisher DA, Howard DM, Burrow JN. 2000. Neurological melioidosis. Acta Trop 74:145-51.
14. Chadwick DR, Ang B, Sitoh YY, Lee CC. 2002. Cerebral melioidosis in Singapore: a review of five cases. Trans R Soc Trop Med Hyg 96:72-6.
15. Schwartzman G, Reddy SA, Berg SH, Currie BJ, Saavedra AP. 2023. Cutaneous melioidosis: An updated review and primer for the dermatologist. J Am Acad Dermatol 89:1201-1208.
16. Currie BJ. 2015. Melioidosis: evolving concepts in epidemiology, pathogenesis, and treatment. Semin Respir Crit Care Med 36:111-25.
17. Price EP, Viberg LT, Kidd TJ, Bell SC, Currie BJ, Sarovich DS. 2018. Transcriptomic analysis of longitudinal *Burkholderia pseudomallei* infecting the cystic fibrosis lung. Microb Genom 4:465 14.
18. Currie BJ, Jacups SP. 2003. Intensity of rainfall and severity of melioidosis, Australia. Emerg Infect Dis 9:1538-42.
19. Chantratita N, Wuthiekanun V, Boonbumrung K, Tiyawisutsri R, Vesaratchavest M, Limmathurotsakul D, Chierakul W, Wongratanacheewin S, Pukritiyakamee S, White NJ, Day NP, Peacock SJ. 2007. Biological relevance of colony morphology and phenotypic switching by *Burkholderia pseudomallei*. J Bacteriol 189:807-17.
20. Vial L, Groleau MC, Lamarche MG, Filion G, Castonguay-Vanier J, Dekimpe V, Daigle F, Charette SJ, Deziel E. 2010. Phase variation has a role in *Burkholderia ambifaria* niche adaptation. ISME J 4:49-60.
21. Mariappan V, Barathan M, Zulpa AK, Vadivelu J, Vellasamy KM. 2023. Small colony variants of *Burkholderia pseudomallei*: alteration of the virulence factors. Journal of Taibah University for Science 17:2244657.
22. Haussler S, Rohde M, Steinmetz I. 1999. Highly resistant *Burkholderia pseudomallei* small colony variants isolated in vitro and in experimental melioidosis. Med Microbiol Immunol 188:91-7.
23. Coulon PML, Groleau MC, Hachani A, Padula MP, Stinear TP, Deziel E. 2025. Quorum sensing and DNA methylation play active roles in clinical *Burkholderia* phase variation. J Bacteriol 207:e0053124.
24. Coulon PML, Agnoli K, Myers GSA. 2025. Colony morphotype variation in *Burkholderia*: implications for success of applications and therapeutics. J Bacteriol 207:e0052124.
25. Chantratita N, Tandhavanant S, Wikraiphat C, Trunck LA, Rholl DA, Thanwisai A, Saiprom N, Limmathurotsakul D, Korbsrisate S, Day NP, Schweizer HP, Peacock SJ. 2012. Proteomic analysis of colony morphology variants of *Burkholderia pseudomallei* defines a role for the arginine deiminase system in bacterial survival. J Proteomics 75:1031-42.
26. Wikraiphat C, Saiprom N, Tandhavanant S, Heiss C, Azadi P, Wongsuvan G, Tuanyok A, Holden MT, Burtnick MN, Brett PJ, Peacock SJ, Chantratita N. 2015. Colony morphology variation of *Burkholderia pseudomallei* is associated with antigenic variation and O-polysaccharide modification. Infect Immun 83:2127-38.
27. Bernhards RC, Cote CK, Amemiya K, Waag DM, Klimko CP, Worsham PL, Welkos SL. 2017. Characterization of in vitro phenotypes of *Burkholderia pseudomallei* and *Burkholderia mallei* strains potentially associated with persistent infection in mice. Arch Microbiol 199:277-301.
28. Al-Maleki AR, Vellasamy KM, Mariappan V, Venkatraman G, Tay ST, Vadivelu J. 2020. Transcriptome analysis of *Burkholderia pseudomallei* SCV reveals an association with virulence, stress resistance and intracellular persistence. Genomics 112:501-512.

29. Austin CR, Goodyear AW, Bartek IL, Stewart A, Sutherland MD, Silva EB, Zweifel A, Vitko NP, Tuanyok A, Highnam G, Mittelman D, Keim P, Schweizer HP, Vazquez-Torres A, Dow SW, Voskuil MI. 2015. A *Burkholderia pseudomallei* colony variant necessary for gastric colonization. mBio 6:e02462--14.
30. Gassiep I, Chatfield MD, Permana B, Burnard D, Bauer MJ, Cuddihy T, Forde BM, Mayer-Coverdale J, Norton RE, Harris PNA. 2024. The Genomic Epidemiology of Clinical *Burkholderia pseudomallei* Isolates in North Queensland, Australia. Pathogens 13:584.
31. Chapalain A, Vial L, Laprade N, Dekimpe V, Perreault J, Deziel E. 2013. Identification of quorum sensing-controlled genes in *Burkholderia ambifaria*. Microbiologyopen 2:226-42.
32. Zlosnik JE, Hird TJ, Fraenkel MC, Moreira LM, Henry DA, Speert DP. 2008. Differential mucoid exopolysaccharide production by members of the *Burkholderia cepacia* complex. J Clin Microbiol 46:1470-3.
33. Louden BC, Haarmann D, Lynne AM. 2011. Use of Blue Agar CAS Assay for Siderophore Detection. J Microbiol Biol Educ 12:51-3.
34. Buxton R. 2005. Blood agar plates and hemolysis protocols. American Society for Microbiology 15:1-9.
35. Gaio D, Anantanawat K, To J, Liu M, Monahan L, Darling AE. 2022. Hackflex: low-cost, high-throughput, Illumina Nextera Flex library construction. Microb Genom 8.
36. De Coster W, D'Hert S, Schultz DT, Cruts M, Van Broeckhoven C. 2018. NanoPack: visualizing and processing long-read sequencing data. Bioinformatics 34:2666-2669.
37. Chen S. 2023. Ultrafast one-pass FASTQ data preprocessing, quality control, and deduplication using fastp. Imeta 2:e107.
38. Wick RR, Howden BP, Stinear TP. 2025. Autocycler: long-read consensus assembly for bacterial genomes. bioRxiv doi:10.1101/2025.05.12.653612:2025.05.12.653612.
39. Bouras G, Judd LM, Edwards RA, Vreugde S, Stinear TP, Wick RR. 2024. How low can you go? Short-read polishing of Oxford Nanopore bacterial genome assemblies. Microb Genom 10.
40. Zimin AV, Salzberg SL. 2020. The genome polishing tool POLCA makes fast and accurate corrections in genome assemblies. PLoS Comput Biol 16:e1007981.
41. Schwengers O, Jelonek L, Dieckmann MA, Beyvers S, Blom J, Goesmann A. 2021. Bakta: rapid and standardized annotation of bacterial genomes via alignment-free sequence identification. Microb Genom 7.
42. Wick RR, Judd LM, Gorrie CL, Holt KE. 2017. Unicycler: Resolving bacterial genome assemblies from short and long sequencing reads. PLoS Comput Biol 13:e1005595.
43. Seemann T. 2015. Snippy: rapid haploid variant calling and core SNP phylogeny. GitHub Available at: github com/tseemann/snippy.
44. Wright PR, Georg J, Mann M, Sorescu DA, Richter AS, Lott S, Kleinkauf R, Hess WR, Backofen R. 2014. CopraRNA and IntaRNA: predicting small RNA targets, networks and interaction domains. Nucleic Acids Res 42:W119-23.
45. Mathews DH, Disney MD, Childs JL, Schroeder SJ, Zuker M, Turner DH. 2004. Incorporating chemical modification constraints into a dynamic programming algorithm for prediction of RNA secondary structure. Proc Natl Acad Sci U S A 101:7287-92.
46. Kong AT, Leprevost FV, Avtonomov DM, Mellacheruvu D, Nesvizhskii AI. 2017. MSFragger: ultrafast and comprehensive peptide identification in mass spectrometry-based proteomics. Nat Methods 14:513-520.

47. Huber W, von Heydebreck A, Sultmann H, Poustka A, Vingron M. 2002. Variance stabilization applied to microarray data calibration and to the quantification of differential expression. Bioinformatics 18 Suppl 1:S96-104.
48. Coombs KM, Berard A, Xu W, Krokhin O, Meng X, Cortens JP, Kobasa D, Wilkins J, Brown EG. 2010. Quantitative proteomic analyses of influenza virus-infected cultured human lung cells. J Virol 84:10888-906.
49. Kammers K, Cole RN, Tiengwe C, Ruczinski I. 2015. Detecting Significant Changes in Protein Abundance. EuPA Open Proteom 7:11-19.
50. Johnson M, Zaretskaya I, Raytselis Y, Merezhuk Y, McGinnis S, Madden TL. 2008. NCBI BLAST: a better web interface. Nucleic Acids Res 36:W5-9.
51. Huerta-Cepas J, Szklarczyk D, Heller D, Hernandez-Plaza A, Forslund SK, Cook H, Mende DR, Letunic I, Rattei T, Jensen LJ, von Mering C, Bork P. 2019. eggNOG 5.0: a hierarchical, functionally and phylogenetically annotated orthology resource based on 5090 organisms and 2502 viruses. Nucleic Acids Res 47:D309-D314.
52. Raivo K. 2025. pheatmap: Pretty Heatmaps. .
53. Team RDC. 2018. R: A language and environment for statistical computing.
54. Sayers EW, Bolton EE, Brister JR, Canese K, Chan J, Comeau DC, Connor R, Funk K, Kelly C, Kim S, Madej T, Marchler-Bauer A, Lanczycki C, Lathrop S, Lu Z, Thibaud-Nissen F, Murphy T, Phan L, Skripchenko Y, Tse T, Wang J, Williams R, Trawick BW, Pruitt KD, Sherry ST. 2022. Database resources of the national center for biotechnology information. Nucleic Acids Res 50:D20-D26.
55. Sayers EW, Cavanaugh M, Clark K, Ostell J, Pruitt KD, Karsch-Mizrachi I. 2019. GenBank. Nucleic Acids Res 47:D94-D99.
56. Perez-Riverol Y, Bai J, Bandla C, Garcia-Seisdedos D, Hewapathirana S, Kamatchinathan S, Kundu DJ, Prakash A, Frericks-Zipper A, Eisenacher M, Walzer M, Wang S, Brazma A, Vizcaino JA. 2022. The PRIDE database resources in 2022: a hub for mass spectrometry-based proteomics evidences. Nucleic Acids Res 50:D543-D552.
57. Gierok P, Kohler C, Steinmetz I, Lalk M. 2016. *Burkholderia pseudomallei* Colony Morphotypes Show a Synchronized Metabolic Pattern after Acute Infection. PLoS Negl Trop Dis 10:e0004483.
58. Vander Broek CW, Stevens JM. 2017. Type III Secretion in the Melioidosis Pathogen *Burkholderia pseudomallei*. Front Cell Infect Microbiol 7:255.
59. Chen Y, Wong J, Sun GW, Liu Y, Tan GY, Gan YH. 2011. Regulation of type VI secretion system during *Burkholderia pseudomallei* infection. Infect Immun 79:3064-73.
60. Chieng S, Mohamed R, Nathan S. 2015. Transcriptome analysis of *Burkholderia pseudomallei* T6SS identifies Hcp1 as a potential serodiagnostic marker. Microb Pathog 79:47-56.
61. Gong L, Cullinane M, Treerat P, Ramm G, Prescott M, Adler B, Boyce JD, Devenish RJ. 2011. The *Burkholderia pseudomallei* type III secretion system and BopA are required for evasion of LC3-associated phagocytosis. PLoS One 6:e17852.
62. Lennings J, West TE, Schwarz S. 2018. The *Burkholderia* Type VI Secretion System 5: Composition, Regulation and Role in Virulence. Front Microbiol 9:3339.
63. Majerczyk C, Schneider E, Greenberg EP. 2016. Quorum sensing control of Type VI secretion factors restricts the proliferation of quorum-sensing mutants. Elife 5:e14712.
64. Sun GW, Chen Y, Liu Y, Tan GY, Ong C, Tan P, Gan YH. 2010. Identification of a regulatory cascade controlling Type III Secretion System 3 gene expression in *Burkholderia pseudomallei*. Mol Microbiol 76:677-89.

65. Toesca IJ, French CT, Miller JF. 2014. The Type VI secretion system spike protein VgrG5 mediates membrane fusion during intercellular spread by pseudomallei group *Burkholderia* species. Infect Immun 82:1436-44.
66. Treerat P, Alwis P, D'Cruze T, Cullinane M, Vadivelu J, Devenish RJ, Prescott M, Adler B, Boyce JD. 2015. The *Burkholderia pseudomallei* Proteins BapA and BapC Are Secreted TTSS3 Effectors and BapB Levels Modulate Expression of BopE. PLoS One 10:e0143916.
67. Warawa J, Woods DE. 2005. Type III secretion system cluster 3 is required for maximal virulence of *Burkholderia pseudomallei* in a hamster infection model. FEMS Microbiol Lett 242:101-8.
68. Kespichayawattana W, Rattanachetkul S, Wanun T, Utaisincharoen P, Sirisinha S. 2000. *Burkholderia pseudomallei* induces cell fusion and actin-associated membrane protrusion: a possible mechanism for cell-to-cell spreading. Infect Immun 68:5377-84.
69. Khoo JS, Chai SF, Mohamed R, Nathan S, Firdaus-Raih M. 2012. Computational discovery and RT-PCR validation of novel *Burkholderia* conserved and *Burkholderia pseudomallei* unique sRNAs. BMC Genomics 13 Suppl 7:S13.
70. Mohd-Padil H, Damiri N, Sulaiman S, Chai SF, Nathan S, Firdaus-Raih M. 2017. Identification of sRNA mediated responses to nutrient depletion in *Burkholderia pseudomallei*. Sci Rep 7:17173.
71. Al-Maleki AR, Mariappan V, Vellasamy KM, Tay ST, Vadivelu J. 2015. Altered Proteome of *Burkholderia pseudomallei* Colony Variants Induced by Exposure to Human Lung Epithelial Cells. PLoS One 10:e0127398.
72. Harland DN, Chu K, Haque A, Nelson M, Walker NJ, Sarkar-Tyson M, Atkins TP, Moore B, Brown KA, Bancroft G, Titball RW, Atkins HS. 2007. Identification of a LolC homologue in *Burkholderia pseudomallei*, a novel protective antigen for melioidosis. Infect Immun 75:4173-80.
73. Price EP, Sarovich DS, Mayo M, Tuanyok A, Drees KP, Kaestli M, Beckstrom-Sternberg SM, Babic-Sternberg JS, Kidd TJ, Bell SC, Keim P, Pearson T, Currie BJ. 2013. Within-host evolution of *Burkholderia pseudomallei* over a twelve-year chronic carriage infection. mBio 4.
74. Vipond J, Kane J, Hatch G, McCorrison J, Nierman WC, Losada L. 2013. Sequence Determination of *Burkholderia pseudomallei* Strain NCTC 13392 Colony Morphology Variants. Genome Announc 1:e00925--13.
75. Le Guillouzer S, Groleau MC, Mauffrey F, Deziel E. 2020. ScmR, a Global Regulator of Gene Expression, Quorum Sensing, pH Homeostasis, and Virulence in *Burkholderia thailandensis*. J Bacteriol 202.
76. Mao D, Bushin LB, Moon K, Wu Y, Seyedsayamdost MR. 2017. Discovery of scmR as a global regulator of secondary metabolism and virulence in *Burkholderia thailandensis* E264. Proc Natl Acad Sci U S A 114:E2920-E2928.

Figures

Figure 1 Characterization of Bp isolates by colony morphology and phenotypes. A) Bp isolates grown on CRLA or Ashdown agar for 3 days, Roman number represent the type of colony morphology. B) Variant emergence among Bp isolates when grown on various agar for 8 days; arrows targets variants emerging from parental isolates. Note: all rough variants retained a macroscopically wrinkled or dry texture when observed by eye, across media.

Figure 2 Proteomic profile of Bp isolates by comparing smooth to rough colonies. Heatmap showing protein abundance difference, for each Bp isolates for common proteins between isolates.

Figure 3 Cluster of Bp isolates, and their variants based on three -omics layers. A) Individual PCA analysis based on either phenotype (16), genomic (19) or proteomic (1429) variables. B) Integrative PCA analysis using on all genomic and phenotypes variable and top 30 proteins differentiating isolates.

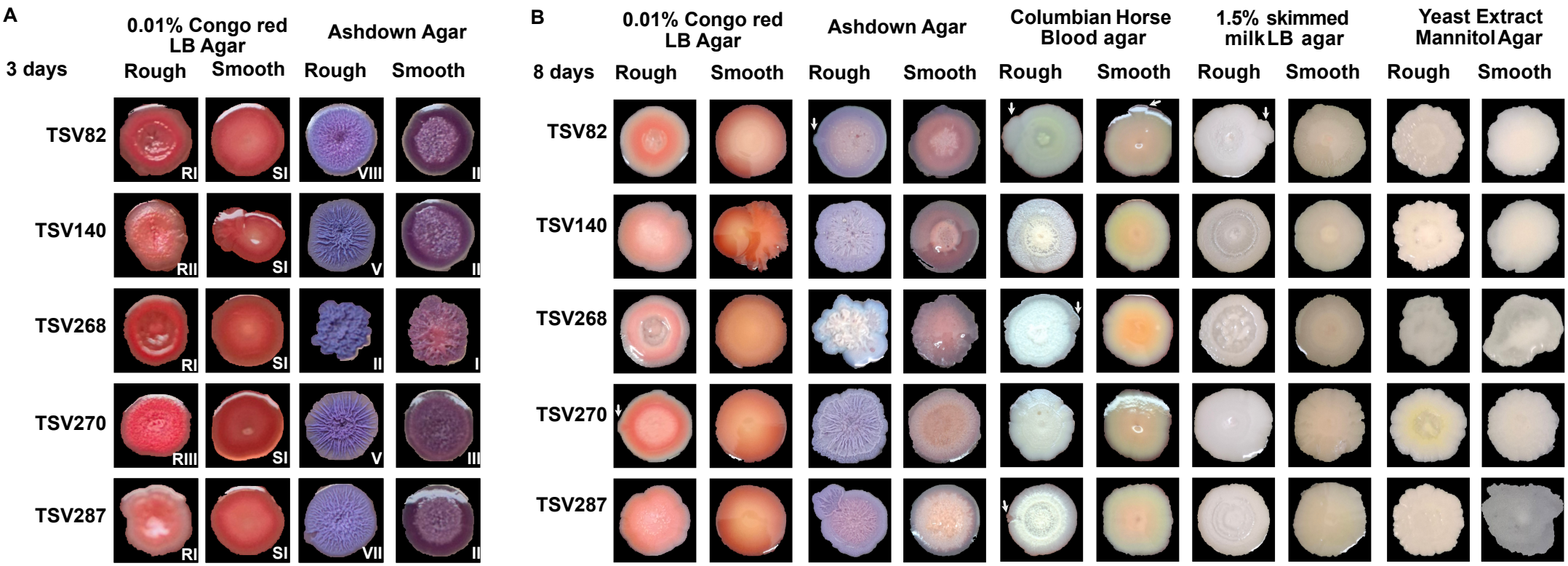
A
3 days
0.01% Congo red LB Agar
Ashdown Agar
Rough
Smooth
Rough
Smooth
TSV82
TSV140
TSV268
TSV270
TSV287
RI
SI
VIII
II
RII
SI
V
II
RI
SI
II
I
RIII
SI
V
III
RI
SI
VII
II
B
8 days
0.01% Congo red LB Agar
Ashdown Agar
Columbian Horse Blood agar
1.5% skimmed milk LB agar
Yeast Extract Mannitol Agar
Rough
Smooth
Rough
Smooth
Rough
Smooth
Rough
Smooth
Rough
Smooth
TSV82
TSV140
TSV268
TSV270
TSV287

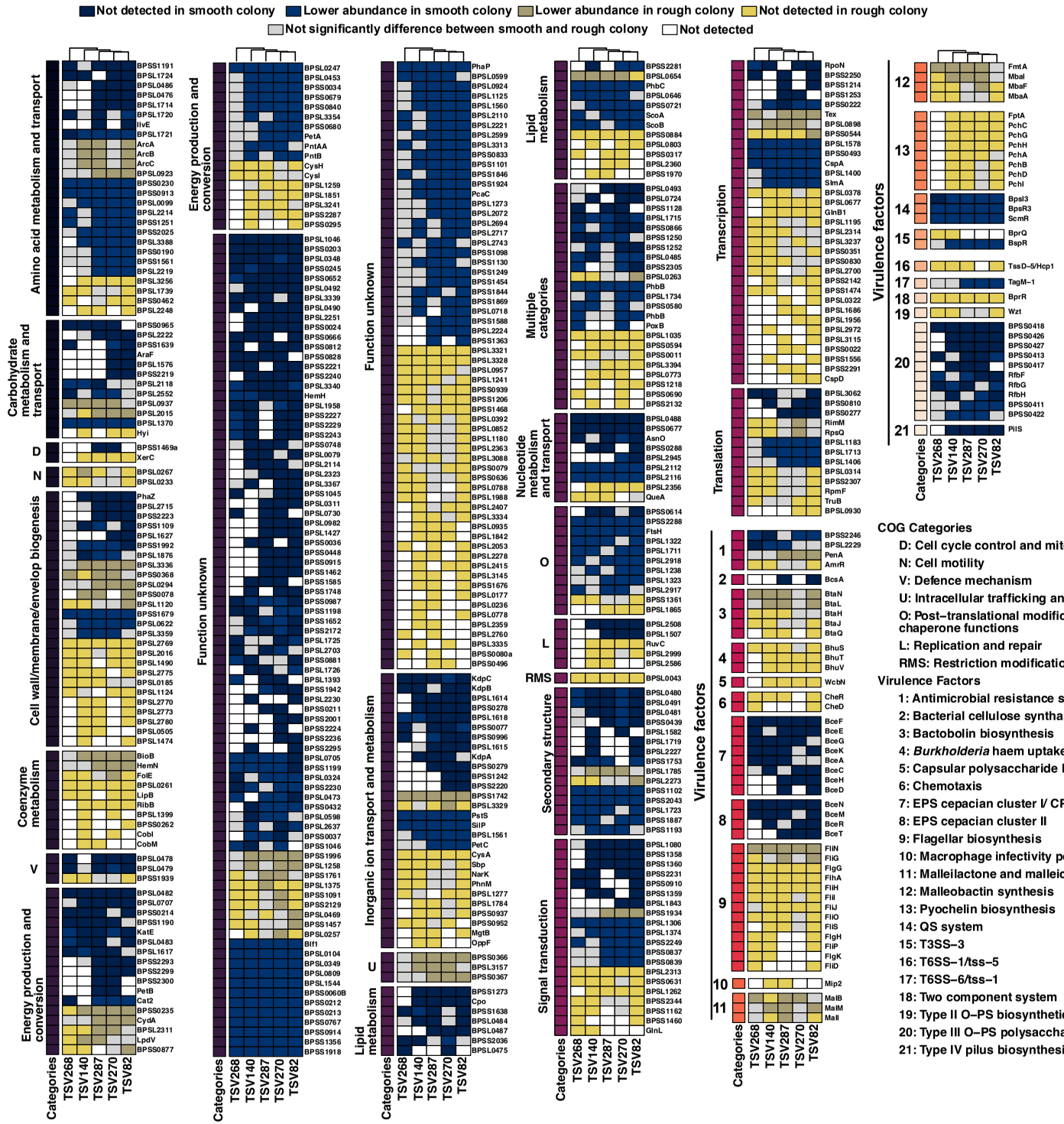

COG Categories

- D: Cell cycle control and mitosis
- N: Cell motility
- V: Defence mechanism
- U: Intracellular trafficking and secretion
- O: Post–translational modification, protein turnover, chaperone functions
- L: Replication and repair
- RMS: Restriction modification system

Virulence Factors

1. Antimicrobial resistance system
2. Bacterial cellulose synthase
3. Bactobolin biosynthesis
4. *Burkholderia* haem uptake
5. Capsular polysaccharide biosynthesis
6. Chemotaxis
7. EPS cepacian cluster I/ CPS III / Type IV O–PS
8. EPS cepacian cluster II
9. Flagellar biosynthesis
10. Macrophage infectivity potentiators (Mips)
11. Malleilactone and malleicyprol biosynthesis
12. Malleobactin synthesis
13. Pyochelin biosynthesis
14. QS system
15. T3SS–3
16. T6SS–1/tss–5
17. T6SS–6/tss–1
18. Two component system
19. Type II O–PS biosynthetic gene cluster
20. Type III O–PS polysaccharide
21. Type IV pilus biosynthesis

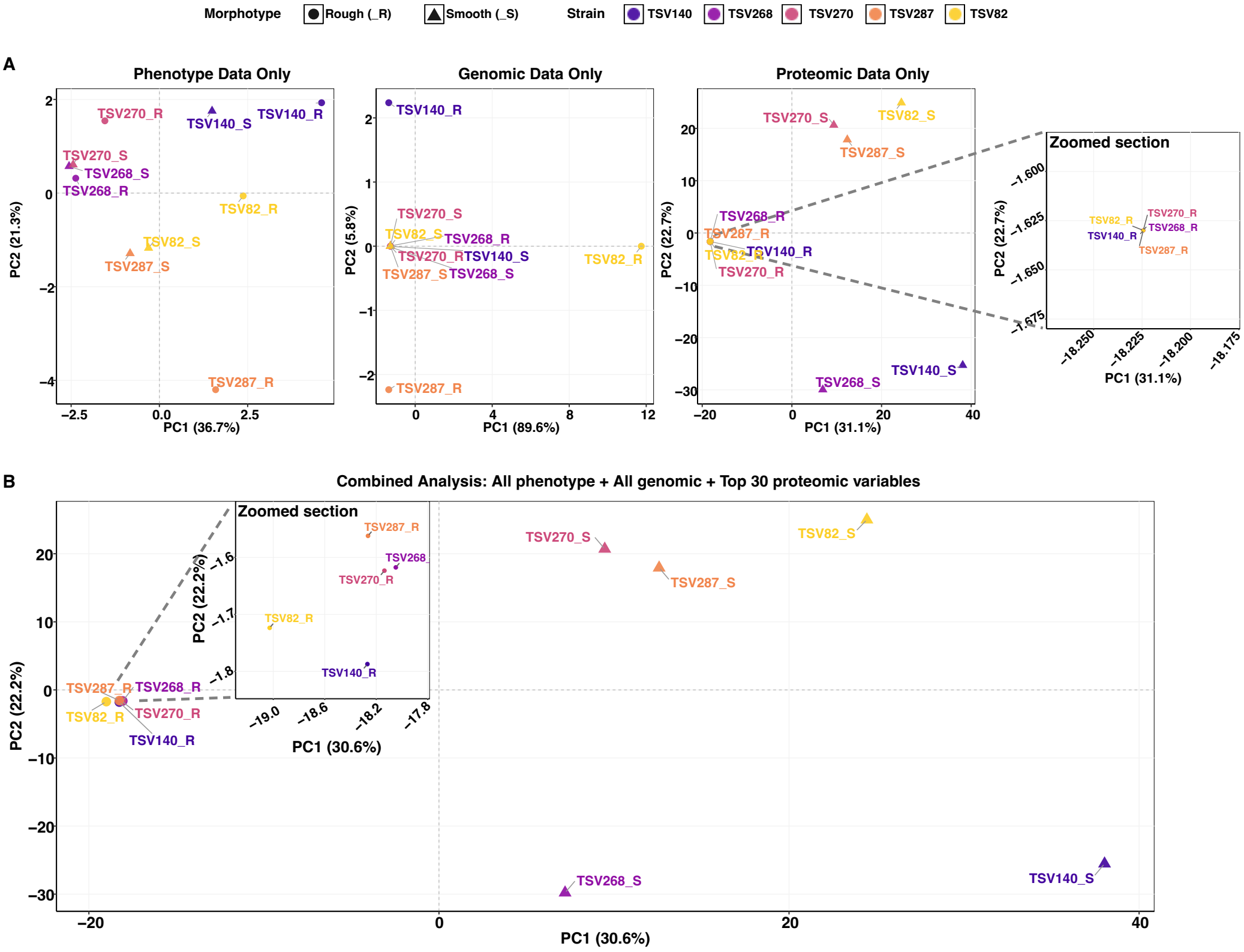
Morphotype
Rough (_R)
Smooth (_S)
Strain
TSV140
TSV268
TSV270
TSV287
TSV82
A
Phenotype Data Only
PC1 (36.7%)
PC2 (21.3%)
Genomic Data Only
PC1 (89.6%)
PC2 (5.8%)
Proteomic Data Only
PC1 (31.1%)
PC2 (22.7%)
Zoomed section
B
Combined Analysis: All phenotype + All genomic + Top 30 proteomic variables
PC1 (30.6%)
PC2 (22.2%)
Zoomed section